Open Access

Journal of Energy and Power Technology

Original Research

An *Ab Initio* Study of Li/Ni-doped Na_xMeO_2 Cathode Material for Na-Ion Batteries

Arianna Massaro [1], Ana B. Muñoz-García [2], Mariarosaria Tuccillo [1, 3], Michele Pavone [1, *], Pier Paolo Prosini [4, *]

1. Università di Napoli Federico II, Dip. Scienze Chimiche, Comp. Univ. Monte Sant'Angelo Via Cintia 21, 80126 Napoli, Italia; E-Mails: arianna.massaro@unina.it; mariartucc@gmail.com; mipavone@unina.it
2. Università di Napoli Federico II, Dip. Fisica "E.Pancini", Comp. Univ. Monte Sant'Angelo Via Cintia 21, 80126 Napoli, Italia; E-Mail: anabelen.munozgarcia@unina.it
3. ISC-CNR, Piazzale Aldo Moro 5, 00185 Roma, Italia
4. ENEA, CR Casaccia TERIN-PSU-ABI, Via Anguillarese 301, 00123 S. Maria di Galeria (Roma), Italia; E-Mail: pierpaolo.prosini@enea.it

* **Correspondence:** Pier Paolo Prosini and Michele Pavone; E-Mails: pierpaolo.prosini@enea.it; mipavone@unina.it

Academic Editor: Zhao Yang Dong

Journal of Energy and Power Technology
2021, volume 3, issue 2
doi:10.21926/jept.2102022

Received: November 02, 2020
Accepted: May 07, 2021
Published: June 10, 2021

Abstract

The current state-of-the-art quantum mechanics methodologies were applied to derive information on the bulk and surface properties of the P2-type layered oxide $Na_{0.85}Li_{0.17}Ni_{0.21}Mn_{0.64}O_2$ (NLNMO), a cathode material. The special quasi-random structure (SQS) approach was employed to identify the arrangement of Li, Ni, and Mn ions in a supercell containing 115 atoms. Both the cell parameters and atomic positions were determined from DFT-PBE+U calculations to highlight specific distortions induced by the dopants (Ni and Li). The analysis of atomic partial charges and atomic magnetic moments revealed that Li has a purely structural role, while Ni and Mn actively participate in both redox processes and

electronic conduction. Using a new surface slab model, the interaction between the layered $Na_{0.85}Li_{0.17}Ni_{0.21}Mn_{0.64}O_2$ (001) surface and the Na ions was examined to identify the most favorable adsorption sites and the possible paths for the migration of the Na ions on the electrode surface.

Keywords
Sodium-ion battery; P2-type layered oxide; special quasi-random structure; surface interaction

1. Introduction

Recently, remarkable progress has been made in the research of new materials for the optimization of high-energy positive electrodes for sodium-ion batteries (NIBs). Several studies have focused on cation engineering in layered oxides with the general formula $NaMeO_2$ (Sodium 3d metal oxides) since structural and electrochemical properties of these materials can be easily tuned and improved via ion doping at the metal (Me) site [1−10]. Among these materials, the P2-type layered oxide with formula ($Na_{2/3}Ni_{1/3}Mn_{2/3}O_2$) has drawn significant attention as a cathode material for NIBs because of its high operating voltage of ∼3.8V and large specific capacity of ∼173 mAh g^{-1} (one of the highest energy densities documented so far among the transition metal (TM) oxides from P2-type layered oxides class) [11]. $Na_{2/3}Ni_{1/3}Mn_{2/3}O_2$, a sodium layered cathode material is stable in the ambient atmosphere, unlike most $NaMeO_2$ materials that show an enhanced hygroscopic character. Other P2-type metal oxides need to be protected immediately after the high-temperature (850–950 °C) sintering procedure. Handling of $Na_{2/3}Ni_{1/3}Mn_{2/3}O_2$ is rather easier due to phase stability issues. The synthesis involves a simple sintering process followed by natural cooling in the air. This process offers several remarkable advantages in practical day-to-day manufacturing, thereby making $Na_{2/3}Ni_{1/3}Mn_{2/3}O_2$ a very promising cathode candidate for application in high-energy SIBs. The crystal structure of the Na_xMeO_2 family of materials was first described by Delmas *et al*. in the early 1980s [12] and subsequently illustrated by Zhang *et al.* [13]. Generally, one layer of octahedral MeO_6 units is alternated with Na ions. The most common lattices are usually labeled with P and O letters, indicating prismatic and octahedral sites of the alkali metal coordination, respectively. These letters are followed by the number of transition metal (TM) layers in the overlay repeat unit (*i.e.,* 2 or 3). **Figure 1** shows a schematic illustration of P2, P3, O2, and O3 crystal structures in Na_xMeO_2 [14]. In P2-type, all the Na ions are accommodated in prismatic sites, and the oxygen ions are stacked in an "ABBA" fashion. In the O3 structure, the Na ions reside in octahedral sites between the TM layers, and the arrangement of the oxygen atoms is in "ABCABC" fashion. Sodium extraction from O3- and P2-type structures, occurring after electrochemical cycling, generally induces phase transitions. The gliding of MeO_2 slabs in O3- and P2-phases can help in the formation of prismatic or octahedral sites upon desodiation, leading to O3→P3 or P2→O2 transitions, respectively. The phase transition from P3/O3-type to the P2-type phase is not observed as it requires a higher-temperature environment to break and reform Me-O bonds (Me = transition metal). To our knowledge, some studies reported OP4-type as another possible phase for layered $NaMeO_2$ systems that can be stabilized at high voltage. This type has generally been observed for Cobalt-based

sodium layered oxides [15-19], whereas only P2-O2/O3-P3 phase transitions have been reported in the case of NLNMO kind of materials [20]. Despite these structural issues, the P2-types have shown greater power performance than the O3-type analogues because of the wide diffusion paths for Na ions [20]. Previous studies have shown that the P2 structure persists until x decreases to ~1/3 (corresponding to a charge voltage of ~4.2V). At this point, O2-type stacking defects begin to appear, leading to the coexistence of both P2 and O2 phases when Na content is significantly reduced (for x < 1/3). The P2→O2 phase transformation upon Na extraction has been widely observed as the primary cause for severe material degradation and huge capacity loss. Several studies have indicated the possibility of such structural evolution in terms of formation energies [21]. Few studies have reported that phase transitions could be established through the formation of ordered superstructures involving the Na^+/vacancy ratio, which could lower the Na^+ diffusion coefficient resulting in sluggish Na transport and poor electrochemical efficiency. Also, Na^+/vacancy disordering ensures fast Na^+ mobility in P2-type compounds [22]. Decomposition of the oxidizable electrolyte is another problem related to high working voltage conditions since it decreases the Coulombic efficiency (CE). Upon discharge, the reduction of Mn^{4+} can lead to the formation of Mn^{3+} ions that are soluble in the electrolyte, with poor cyclic stability. Reduction of Mn^{4+} contributes to the capacity exhibited by the material when the cell voltage is brought to 1.6 V vs. Na/Na^+, while upon charging, only Ni^{2+} is oxidized.

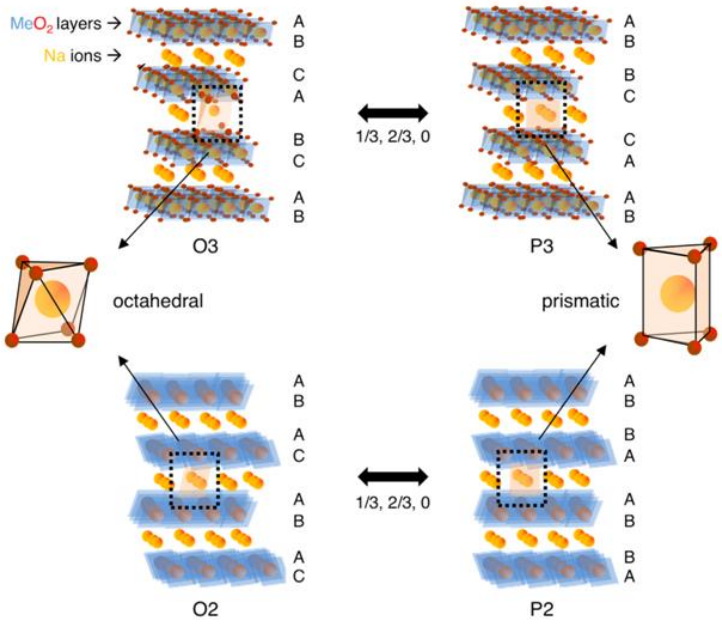

Figure 1 Schematic representation of layered transition metal oxides with general formula Na_xMeO_2. The arrows indicate phase transition processes induced by sodium extraction. Adapted from Ref. [14].

The above discussion clarifies that the electrochemical performance of $Na_{2/3}Ni_{1/3}Mn_{2/3}O_2$ can be improved by

(i) suppressing the structural transformation P2→O2;
(ii) increasing the Na^+ /vacancy ratio;
(iii) avoiding or reducing the participation of the redox pair Mn^{4+}/Mn^{3+} ions, and

(iv) inhibiting the decomposition of the electrolytes.

Numerous approaches have been suggested to improve the performance of P2-type sodium compounds. The replacement of sodium with other alkali metal ions (*e.g.,* lithium) or alkaline-earth ions (*e.g.,* magnesium) has been one of the most studied strategies. It is recognized that lithium ions used as dopants preferably occupy the TM layers since the large size of sites in the Na layers cannot allow the Li ions to remain stable. The typical plateau seen in the voltage profiles upon charge/discharge gradually disappears after the introduction of Li ions, suggesting that the reaction mechanism changes from a series of phase transition reactions to solid solution-like behavior. The presence of Li ions can prevent the phase transition with a stabilizing effect of the P2 structure over a wide range of Na ions concentrations (voltage range 2.0–4.4 V), with varying reticular parameters, thereby improving the overall performance [23-25]. The function of Li in stabilizing the structure may be closely related to the migration of Li ions from the TM layer to the Na layer that occurs only at high voltage. The higher electropositive Li ions that migrate to the Na layers can hold the adjacent TM layers together, thereby inhibiting both the flow of the oxygen layer and the phase transformation [26].

The charge/discharge dynamics, the specific role of each constituent element in the material, the electrical conduction properties, and the surface chemistry of these electrodes present several fundamental questions, despite numerous studies carried out so far. Density functional theory (DFT) calculations have proven to be a useful technique for evaluating the thermodynamic, structural, and kinetic properties of manganese oxide (MnO_2) with monoclinic [27] and spinel structure [28] for their use as cathode materials for NIBs. Therefore, we applied an advanced quantum mechanics (QM) method based on DFT [29, 30] and combined with a statistical approach to evaluate the $Na_{0.85}Li_{0.17}Ni_{0.21}Mn_{0.64}O_2$ (NLNMO) material as P2-type layered oxide with the promising application as a cathode electrode in NIBs [31]. The choice of NLNMO material was driven by the increasing interest in Li-doped $NaMeO_2$ materials, owing to the enhanced capacity in a wide voltage range ensured with Me = Ni, Mn (160 mAh g^{-1} within 2.0–4.5 V range) [20, 24] and the excellent rate capabilities enabled by Li substitution (single smooth voltage profile) [31]. Despite these encouraging improvements, an in-depth analysis of Na ions intercalation and diffusion mechanisms in such innovative materials is still lacking. Possibly, the current study will set the direction for future works to develop and optimize high-energy cathode materials in effective NIB devices.

2. Materials and Methods

To build a realistic structural model for NLNMO bulk, we applied a statistical method that could simulate a disordered distribution of Mn/Ni/Li atoms within the Me-based layers of the material. The special quasi-random structure (SQS) method allows modeling of a random solid solution in a supercell of the desired size by building periodic structures whose properties simulate those of random material, *i.e.,* at the limit of a perfectly random alloy (considering the two- and three-body correlation functions in a random alloy, through the interactions of each element grid with the nearest neighbor, and so on) [32, 33]. The SQS model represents the best choice of a supercell with a random distribution of TM centers in the lattice obtained to maximize the configurational entropy within the limit of the given supercell. For sodium distribution over (e) (coordinated to the octahedron edge) and (f) (coordinated to the octahedron face) sites, we considered the occupancy ratio as previously reported in the literature and placed Na atoms accordingly [34, 35]. We applied

the solid-state physics code Vienna *ab-initio* simulation package (VASP) that performs first-principles quantum-mechanics calculations within DFT using the projector augmented wave (PAW) pseudopotentials and plane waves basis set with periodic boundary conditions. The spin-polarized DFT calculations were done using the Perdew-Burke-Ernzerhof (PBE) exchange-correlation functional based on the generalized gradient approximation (GGA). The DFT functionals showed significant problems of self-interaction error (SIE) with localized electrons. Since we dealt with highly localized *d* electrons of Mn and Ni, the DFT+U scheme was employed. The DFT+U method is a more convenient method to rectify the SIE compared to theoretical approaches based on different hybrid functionals. The DFT+U method enabled us to gain useful theoretical insights into the electronic structures of complex materials and interfaces with good accuracy/computational cost ratio [36–38]. The basic idea was to analyze the strong Coulombic interaction of localized electrons with the Hubbard model, which is based on the U (Exchange) and J (Coulomb) parameters and can be derived either from *ab initio* calculations or bandgap values measured experimentally. Herein, we used U-J = 4 eV for *d* electrons of both Mn and Ni. Kinetic energy cut-off of 750 eV and a 2 × 3 × 4 Γ-centered *k*-points grid to converge the plane-wave basis set.

3. Results and Discussion

We first developed the structural model of NLNMO through the SQS approach, starting with a 5 × 3 × 1 supercell of 115 atoms. The geometry optimization of both cell parameters and atomic positions was done to obtain the minimum-energy structure at the PBE+U level of theory. **Figure 2** shows the corresponding energy structure with a volume of 82.5 Å^3/fu that is in good agreement with the experimental value of ~80.4 Å^3 obtained with X-ray diffraction (XRD) (See **Table 1** for structural details) [31]. Figure 2 also shows the electronic properties of the bulk of the material. The nature of the electronic states close to Fermi Energy allows the identification of the responsible or involved species in the electronic conduction. It can be concluded that both valence and conduction bands are dominated by Ni (black) and Mn (purple) *d* states that are strongly hybridized with O *p* states (red), while Na and Li *s* states (yellow and green, respectively) are rather absent in the energy range around E_F. This showed that only Ni, Mn, and O atoms play the electrochemically active role in NLNMO cathode material.

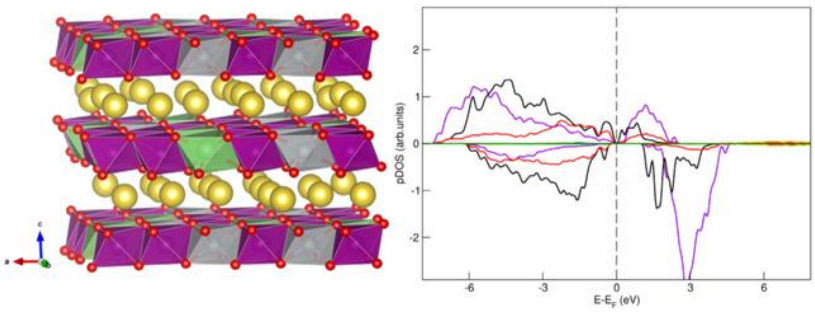

Figure 2 (left) PBE+U minimum-energy structure of NLNMO with SQS distribution of Mn/Ni/Li species; Color codes: Na (yellow), Mn (purple), Ni (grey), and Li (green). **(right)** Atom-and angular momentum-spin projected density of states (pDOS). Color codes: Na *s* states (yellow), Mn *d* states (purple), Ni *d* states (black), and Li *s* states (green).

The analysis of the atomic partial charges and magnetic moments validated the qualitative results obtained by pDOS. Li showed zero magnetic moment, while Ni and Mn had an average magnetic moment of 1.14 μB and 3.21 μB, respectively. These results corresponded to the X-ray absorption near edge structure (XANES) analysis of the material, which indicated the presence of Ni (II) and high spin Mn (III) [31].

Table 1 PBE+U lattice parameters of NLNMO. Experimental values are reported for comparison. The computed value is the multiple of the experimental one, considering the 5 × 3 × 1 size of the supercell.

	a (Å)	c (Å)	γ (°)
current study	14.748	11.045	120
exp [31]	14.450	11.063	120

In order to obtain structural information, we analyzed the distances between the cations and the oxide anion. **Figure 3** shows the distribution of these distances in the form of a pair distribution function (PDF).

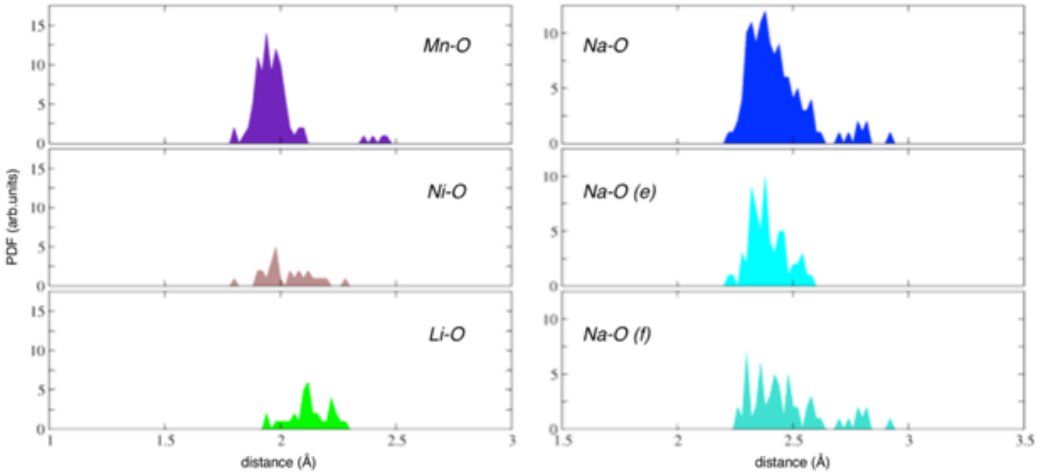

Figure 3 Pair distribution function corresponding to the atom pairs indicated in the legend. In the right panel, the PDF of Na-O distances is decomposed in sodium ions lying in edge (e) and face (f) positions.

The distribution of the distances between the cation and the oxide in the TM layer of Li, Ni, and Mn showed a similar pattern, indicating that the same octahedral coordination is shown by all the cations with oxygen. Li exhibited a slightly longer distance than Ni and Mn. Mn showed a partial elongation of some bonds, according to the Jahn-Teller distortion that is typical for Mn (III) with a high-spin d^4 configuration. Overall, the PDFs confirmed the perfect miscibility of the three cations in the oxide layer and the choice of the SQS approach to building a realistic and robust model. In the case of sodium-oxide distances (Figure 3, right panel), the corresponding PDF showed greater variability, with distances ranging from ~2.2 to ~2.9 Å. By decoupling the two components from the total Na-O PDF, the distribution of distances for the sodium ions lying in (e) and (f) positions were obtained. The intensities of these two PDFs reflected the sodium occupancy in the structural

model, with Na (e)-O distances being more dominant than Na (f)-O ones. The greater variability of the distances was due to the sodium cations in (f) position, while the Na (e) PDF was more compact, demonstrating a higher structuring for these Na sites.

Out of this bulk structure, we cleaved the lattice along the (001) direction to obtain a surface model. An appropriate understanding of the interaction of the Na ion with the NLNMO surface is vital to study the complete characterization of the Na-ion intercalation reaction and the detailed mechanism of Na-ion diffusion occurring at the cathode surface. Our structural model for (001) NLNMO surface had a 5L-slab with a symmetric pattern (two oxide-based terminations) to avoid a strong electrostatic dipole and a 12Å-vacuum layer to avoid fictitious interactions resulting from the periodic boundary conditions (**Figure 4**). Though applied to study different materials, the surface slab approach has not been applied to this kind of electrode. We addressed the Na-(001) NLNMO interaction to the adsorption of one Na ion on two possible sites: Na (e) and Na(f), as depicted in Figure 4. The total sodium concentration was lower than that in the bulk state.

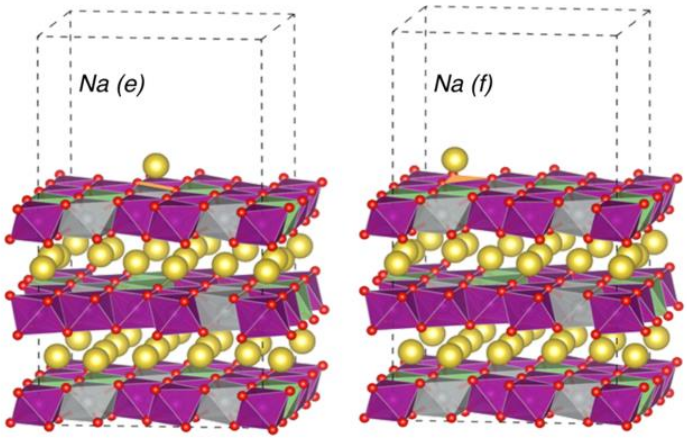

Figure 4 Minimum-energy structures of the Na-adsorbed state on the (001) surface: the two possible positions considered, edge (e) and face (f), are shown, respectively, on the left and the right and are highlighted in orange.

Comparison of Na (e)-and Na (f)-adsorbed systems allowed to identify which site is favored and which site may represent a metastable state along the migration coordinate in the direction parallel to the electrode surface. We observed that after optimizing the Na-adsorbed states, the sodium ions located in position (f) site became slightly more stable compared to the one in position (e). However, the energy difference between these two minima was only 0.15 eV in favor of the (f) site. This was as per the expectations because in the (f) site the positive Na^+ interacts directly with three oxide anions, thereby maximizing the Coulomb interaction between ions with opposite charge, while in the position (e) there were only two neighboring oxide anions. The slightly higher stability of Na(f) sites might also be associated with the larger structural flexibility of these configurations compared to Na (e) ones evident from the wider peaks in the PDF illustrated in Figure 3. Our findings suggested that the sodiation process would commence with Na-adsorption on face sites, and then the complete sodiation will be achieved through the edge ones. Future works should address the Na-Na interaction to unveil the surface activity upon subsequent Na^+ intercalation (*i.e.,* discharging process of NLNMO cathode material till full sodiation is achieved) and also explore Na-NLNMO

interaction on different crystal facets. In this way, the sodium transport process at the electrode surface will be chased with detailed pathways and energetics.

4. Conclusions

This study highlighted the theoretical characterization of the physico-chemical properties of NLNMO as a possible high-energy cathode material for sodium-ion batteries. The material possesses a layered structure where TM oxide layers alternate with Na cations. In the TM oxide layer, both Li and Ni occupy the positions of Mn as substitutional defects. We first defined the methodology to build a realistic structural model of the material. To represent the disordered distribution of Li, Ni, and Mn, the SQS approach was adopted. Through this method, a supercell of the material could be considered where the arrangement of Li, Ni, and Mn is constructed to maximize the configurational entropy of the total system. The sodium cation, in turn, can assume two possible lattice positions differing for the coordination to the oxide anions (on the edge of the octahedron or in the center of the octahedron face). The results showed that the sodium cations in position (f) were slightly less ordered than that in position (e). This structural variability can result in a flat potential energy surface at position (f) and, therefore, a more favorable condition to diffuse. The analysis of the electronic structure showed the mixed nature of the valence and conduction bands that included Mn *d* states, Ni *d* states, and O *p* states, thereby excluding the non-participating Na and Li cations in the electronic conductivity.

In summary, our findings confirmed that lithium has a purely structural role, while nickel and manganese actively participate in both redox processes and electronic conduction. Therefore, the optimum ratio between these elements is crucial to obtain a material with good mechanical stability and enhanced electrical conduction. The optimization of the atomic positions for the surface of the material showed the absence of significant surface reconstruction, thereby demonstrating the stability of the oxide layer. The adsorption of a sodium atom at sites (e) and (f) on top of the (001) surface showed that the face coordination is slightly favored for about 150 meV. This suggested that the sodiation process begins with adsorption on (f) sites, and then the complete sodiation is achieved through the more abundant (e) sites.

Acknowledgments

The computing resources and the related technical support used for this work have been provided by CRESCO/ENEAGRID High Performance Computing infra- structure and its staff [39]; CRESCO/ENEAGRID High Performance Computing infrastructure is funded by ENEA, the Italian National Agency for New Technologies, Energy and Sustainable Economic Development and by Italian and European research programs. See: http://www.cresco.enea.it/english for information.

Author Contributions

Conceptualization, M.P.; Computations, A.M., A.B.M.-G., M.T.; Preparation and revision of the manuscript P.P.P.

Funding

This work was supported by the Italian Ministry of Economic Development through the funds allocated to the "Ricerca Sistema Elettrico" a 2019-2021 three-year implementation plan. Authors acknowledge the European Union (FSE, PON Ricerca e Innovazione 2014–2020, Azione I.1 “Dottorati Innovativi con caratterizzazione Industriale”), for funding a PhD grant to A.M.

Competing Interests

The authors have declared that no competing interests exist.

References

1. Xu JL, Chen JZ, Zhang K, Li NN, Tao L, Wong CP. Na_x(Cu-Fe-Mn)O_2 system as cathode materials for Na-ion batteries. Nano Energy. 2020; 78: 105142.
2. Singh G, Tapia-Ruiz N, del Amo JM, Maitra U, Somerville JW, Armstrong AR, et al. High voltage Mg-doped $Na_{0.67}Ni_{0.3-x}Mg_xMn_{0.7}O_2$ (x = 0.05, 0.1) Na-ion cathodes with enhanced stability and rate capability. Chem Mater. 2016; 28: 5087-5094.
3. Hou PY, Sun YY, Li F, Sun YM, Deng XL, Zhang HZ, et al. A high energy-density P2-$Na_{2/3}[Ni_{0.3}Co_{0.1}Mn_{0.6}]O_2$ cathode with mitigated P2-O2 transition for sodium-ion batteries. Nanoscale. 2019; 11: 2787-2794.
4. Talaie E, Duffort V, Smith HL, Fultz B, Nazar LF. Structure of the high voltage phase of layered P2-$Na_{2/3-z}[Mn_{1/2}Fe_{1/2}]O_2$ and the positive effect of Ni substitution on its stability. Energy Environ Sci. 2015; 8: 2512-2523.
5. Choi JU, Jo JH, Park YJ, Lee KS, Myung ST. Mn-rich P’2-$Na_{0.67}[Ni_{0.1}Fe_{0.1}Mn_{0.8}]O_2$ as high-energy-density and long-life cathode material for sodium-ion batteries. Adv Energy Mater. 2020; 10: 2001346.
6. Yabuuchi N, Kajiyama M, Iwatate J, Nishikawa H, Hitomi S, Okuyama R, et al. P2-type $Na_x[Fe_{1/2}Mn_{1/2}]O_2$ made from earth-abundant elements for rechargeable Na batteries. Nat Mater. 2012; 11: 512-517.
7. Li L, Wang HB, Han WZ, Guo H, Hoser A, Chai YJ, et al. Understanding oxygen redox in Cu-doped P2-$Na_{0.67}Mn_{0.8}Fe_{0.1}Co_{0.1}O_2$ cathode materials for Na-ion batteries. J Electrochem Soc. 2018; 165: A3854.
8. Wang XF, Tamaru M, Okubo M, Yamada A. Electrode properties of P2-$Na_{2/3}Mn_yCo_{1-y}O_2$ as cathode materials for sodium-ion batteries. J Phys Chem C. 2013; 117: 15545-15551.
9. Zhu YE, Qi XG, Chen XQ, Zhou XL, Zhang X, Wei JP, et al. A P2-$Na_{0.67}Co_{0.5}Mn_{0.5}O_2$ cathode material with excellent rate capability and cycling stability for sodium ion batteries. J Mater Chem A. 2016; 4: 11103-11109.
10. de la Llave E, Nayak PK, Levi E, Penki TR, Bublil S, Hartmann P, et al. Electrochemical performance of $Na_{0.6}[Li_{0.2}Ni_{0.2}Mn_{0.6}]O_2$ cathodes with high-working average voltage for Na-ion batteries. J Mater Chem A. 2017; 5: 5858-5864.
11. Yabuuchi N, Kubota K, Dahbi M, Komaba S. Research development on sodium-ion batteries. Chem Rev. 2014; 114: 11636-11682.
12. Delmas C, Fouassier C, Hagenmuller P. Structural classification and properties of the layered oxides. Physica B+C. 1980; 99: 81-85.

13. Zhang JL, Wang WH, Wang W, Wang SW, Li BH. Comprehensive review of P2-type $Na_{2/3}Ni_{1/3}Mn_{2/3}O_2$ a potential cathode for practical application of Na-ion batteries. ACS Appl Mater Interfaces. 2019; 11: 22051-22066.
14. Yabuuchi N, Komaba S. Recent research progress on iron- and manganese-based positive electrode materials for rechargeable sodium batteries. Sci Technol Adv Mater. 2014; 15:4 043501. DOI: 10.1088/1468-6996/15/4/04350
15. Berthelot R, Pollet M, Carlier D, Delmas C. Reinvestigation of the OP4-(Li/Na)CoO_2-layered system and first evidence of the (Li/Na/Na)CoO_2 phase with OPP9 oxygen stacking. Inorg Chem. 2011; 50: 2420-2430.
16. Balsys RJ, Davis RL. The structure of $Li_{0.43}Na_{0.36}CoO_{1.96}$ using neutron powder diffraction. Solid State Ion. 1994; 69: 69-74.
17. Ren Z, Shen JQ, Jiang S, Chen XY, Feng CM, Xu ZA, et al. Enhanced thermopower in an intergrowth cobalt oxide $Li_{0.48}Na_{0.35}CoO_2$. J Phys Condens Matter. 2006; 18: L379.
18. Chen XY, Xu XF, Hu RX, Ren Z, Xu ZA, Cao GH. Synthesis and thermopower measurement of $Li_xNa_yCoO_2$. Acta Phys Sin. 2007; 56: 1627-1631.
19. Bos JW, Hertz JT, Morosan E, Cava RJ. Magnetic and thermoelectric properties of layered $Li_xNa_yCoO_2$. J Solid State Chem. 2007; 180: 3211-3217.
20. Wang PF, You Y, Yin YX, Guo YG. Layered oxide cathodes for sodium-ion batteries: Phase transition air stability and performance. Adv Energy Mater. 2018; 8: 1701912.
21. Lee DH, Xu J, Meng YS. An advanced cathode for Na-ion batteries with high rate and excellent structural stability. Phys Chem Chem Phys. 2013; 15: 3304-3312.
22. Wang PF, Yao HR, Liu XY, Yin YX, Zhang JN, Wen YR, et al. Na^+/vacancy disordering promises high-rate Na-ion batteries. Sci Adv. 2018; 4: eaar6018.
23. Sun JL, Shen JX, Wang TL. Electrochemical Study of $Na_{0.66}Ni_{0.33}Mn_{0.67}Mo_xO_2$ as cathode material for sodium-ion battery. J Alloys Compd. 2017; 709: 481-486.
24. Xu J, Lee DH, Clément RJ, Yu XQ, Leskes M, Pell AJ, et al. Identifying the critical role of Li substitution in P2-$Na_x[Li_yNi_zMn_{1-y-z}]O_2$ ($0 < xyz < 1$) intercalation cathode materials for high-energy Na-ion batteries. Chem Mater. 2014; 26: 1260-1269.
25. Karan NK, Slater MD, Dogan F, Kim D, Johnson CS, Balasubramanian M. Operando structural characterization of the lithium-substituted layered sodium-ion cathode material P2-$Na_{0.85}Li_{0.17}Ni_{0.21}Mn_{0.64}O_2$ by X-ray absorption spectroscopy. J Electrochem Soc. 2014; 161: A1107-A1115.
26. Clement RJ, Bruce PG, Grey CP. Review - manganese based P2-type transition metal oxides as sodium-ion battery cathode materials. J Electrochem Soc. 2015; 162: A2589-A2604.
27. Sudarsanan V, Augustine AM, Vivek C, Ravindran P. Ab-initio based thermodynamic study on α-$NaMnO_2$ for Na-ion battery applications. AIP Conf Proc. 2019; 2115: 030586.
28. Vasileiadis A, Carlsen B, de Klerk NJ, Wagemaker M. Ab initio study of sodium insertion in the λ-Mn_2O_4 and dis/ordered λ-$Mn_{1.5}Ni_{0.5}O_4$ spinels. Chem Mater. 2018; 30: 6646-6659.
29. Kresse G, Hafner J. Ab initio molecular dynamics for open-shell transition metals. Phys Rev B. 1993; 48: 13115.
30. Kresse G, Furthmüller J. Efficient iterative schemes for ab initio total-energy calculations using a plane-wave basis set. Phys Rev B. 1996; 54: 11169.

31. Kim DH, Kang SH, Slater M, Rood S, Vaughey JT, Karan N, et al. Enabling sodium batteries using lithium-substituted sodium layered transition metal oxide cathodes. Adv Energy Mater. 2011; 1: 333-336.
32. Zunger A, Wei SH, Ferreira LG, Bernard JE. Special quasirandom structures. Phys Rev Lett. 1990; 65: 353.
33. Mayer JE, Montroll E. Molecular distribution. J Chem Phys. 1941; 9: 2-16.
34. Yang LF, Li X, Ma XT, Xiong S, Liu P, Tang YZ, et al. Design of high-performance cathode materials with single-phase pathway for sodium ion batteries: A study on P2-$Na_x(Li_yMn_{1-y})O_2$ compounds. J Pow Sour. 2018; 381: 171-180.
35. Fielden R, Obrovac MN. Investigation of the $NaNi_xMn_{1-x}O_2$ ($0 \leq x \leq 1$) system for Na-ion battery cathode materials. J Electrochem Soc. 2015; 162: A453-A459.
36. Muñoz-García AB, Sannino F, Vitiello G, Pirozzi D, Minieri L, Aronne A, et al. Origin and electronic features of reactive oxygen species at hybrid zirconia-acetylacetonate interfaces. ACS Appl Mater Interfaces. 2015; 7: 21662-21667.
37. Muñoz-García AB, Pavone M. Structure and energy level alignment at the dye-electrode interface in p-type DSSCs: New hints on the role of anchoring modes from ab initio calculations. Phys Chem Chem Phys. 2015; 17: 12238-12246.
38. Carella A, Centore R, Borbone F, Toscanesi M, Trifuoggi M, Bella F, et al. Tuning optical and electronic properties in novel carbazole photosensitizers for p-type dye-sensitized solar cells. Electrochim Acta. 2018; 292: 805-816.
39. Ponti G, Palombi F, Abate D, Ambrosino F, Aprea G, Bastianelli T, et al. The role of medium size facilities in the HPC ecosystem: the case of the new CRESCO4 cluster integrated in the ENEAGRID infrastructure. Proceedings of International Conference on High Performance Computing & Simulation; 2014 July 22-25; Bologna, Italy. New York: Institute of Electrical and Electronics Engineers.